Massachusetts Institute of Technology
Kavli Institute for Astrophysics & Space Research
1 Hampshire Street
Cambridge, MA 02139-4307

Tel: 617-253-7277
Fax: 617-253-8084

report

Date: September 6, 2006 6:08 PM

To: ACIS Instrument Team

From: Peter G. Ford, NE80-6071 <pgf@space.mit.edu>

Subject: Version 1.0 of a report relating to SPR 139 (M06080401): "Occasional bias map corruption"

Cc: Chandra SOT <sot@head-cfa.cfa.harvard.edu>

ACIS Instrument Team

1 Introduction

On 08/04/06, OCC reported an anomaly in the bias map for CCD_S2 in OBSID 4111. An examination of all bias maps downlinked from ACIS since the end of OAC yielded 3 other similar anomalies (OBSIDs 6409, 58917, and 6421) in which the pixel values were consistently higher by a few ADU within a limited region which overlapped output node boundaries and which, in three cases, possessed linear boundaries aligned at an angle to the row and column directions.

This anomaly is being tracked by the ACIS SI team as SPR 139.

2 Preliminary Analysis

The anomalous bias map for OBSID 4111 is shown in the left-hand image of Fig. 1, where the relevant node-averaged overclock value has been subtracted from each bias pixel. The first row read out of the CCD is at the top and node A is on the left. Column and row coordinates are shown in the center diagram. The scales beneath the images are in ADUs. The faint ovoids in the bias map are caused by charge blooms in the CCD frames used to create the bias map. The elevated values between columns 498 and 526 are characteristic of this CCD and its DEA video board, but the trapezium-shaped region in the top right is anomalous. Its bias values are ~3 ADU higher than the surrounding pixels, and most peculiarly, it is not restricted to a single node and its straight edges do not lie along row or node boundaries.

The telemetry stream was examined carefully, without finding any evidence of packet dropout or bit corruption. The former would cause one or more consecutive bias map rows to be missing, but since the row indices are transmitted with each packet, this would be reported by the ground software and one or

Figure 1: Left: the bias map for CCD_S2 in OBSID 4111; Center: the location of the artifact; Right: the average of the corner pixels from the 3x3 event islands reported during this run.

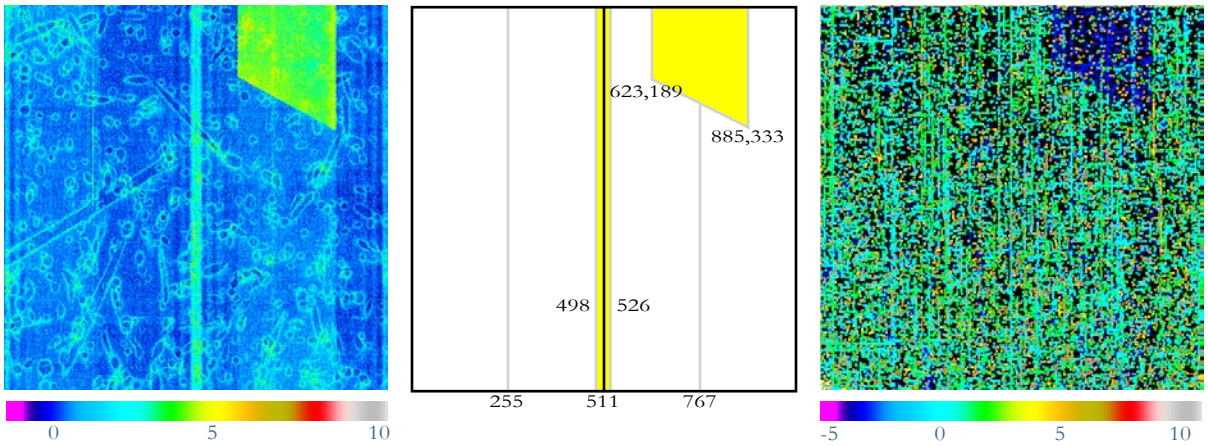

more blank lines would appear in the image. One- or two-bit corruption has been seen occasionally. Since the bias packets are individually compressed by a Huffman algorithm, there is no built-in scheme for locating bit errors, but the result is easily detected by examining the decompressed rows: the pixels following the bit error possess wildly varying values relative to their neighbors in adjoining rows. On several past occasions, we have been able to correct 1- and 2-bit bias packet errors by systematically toggling bits in the corrupted packet, decompressing it, and searching for the minimum variance of the column values. In the present case, each telemetry packet contained 10 independently compressed rows, thereby removing from consideration anything that was done to the bias map after it left the instrument.

The right hand image in Fig. 1 shows the average values of the corner pixels from the x-ray events reported from this run. Since ACIS was in timed-exposure 5x5 mode, 25 pixel values were recorded for each event candidate, and the lowest 8 values were averaged, after bias subtraction, to generate the image in this figure. The anomalous area in the bias map is clearly reproduced in the corner average image, but in reverse. When the corner pixels were normalized by a different CCD_S2 bias map made shortly before OBSID 4111 but with the same parameters, no anomalously low region could be detected, implying that the artifact was restricted to the bias map itself—the event pixels were free of it.

Figure 2: Distribution of bias values in OBSID 4111, S2, for pixels within and outside the anomalous region.

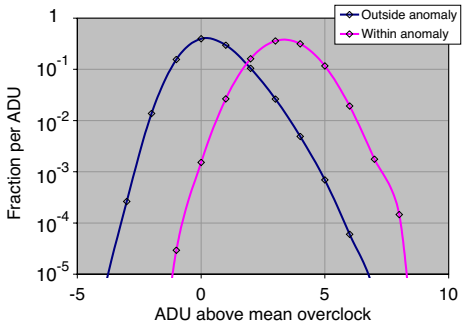

Fig. 2 shows the distribution of pixel values (after subtracting node-averaged overclocks) inside and outside the anomalous region in the bias map. The shape of the latter (blue curve) is consistent with the histograms that were generated from laboratory CCDs and proto-flight software while developing the bias algorithms several years prior to launch and described in Applicable Document 3. The distribution of pixel values in the anomalous region (magenta curve) is slightly more symmetric, with less of a high-energy tail.

The next step was to systematically examine *all* ACIS bias maps to see whether there had been other instances of similar anomalies. The maps were processed in a fashion similar to the left hand image in Fig. 1, *i.e.*, the node-averaged overclock values were subtracted from each bias value, spatially averaged to 256 rows and columns, and saved as a GIF image with a strong colormap stretch between –2 and +10 ADU. The output files were sorted (a) by mode (timed-exposure *vs.* continuously clocked), (b) by CCD, and (c) by epoch. They were then displayed as an array of small squares by the *xv* image browser. Since most maps from a given CCD were very similar, those that weren't were readily discernible. Out of 29673 maps inspected to date (28695 timed exposure, 978 continuously clocked), 102 maps from 73 science runs showed some anomaly (see Appendix A), but all but 4 had a simple explanation, *viz.*

- 43 maps were corrupted due to telemetry dropouts
- 20 maps were generated by non-standard calibration modes, *e.g.*, squeegee, cuckoo.
- 31 maps were corrupted due to excessive background radiation
- 4 maps contained an optical image of the planet Jupiter

Figure 3: The four anomalous bias maps: color represents pixel value in ADU above average overclock.

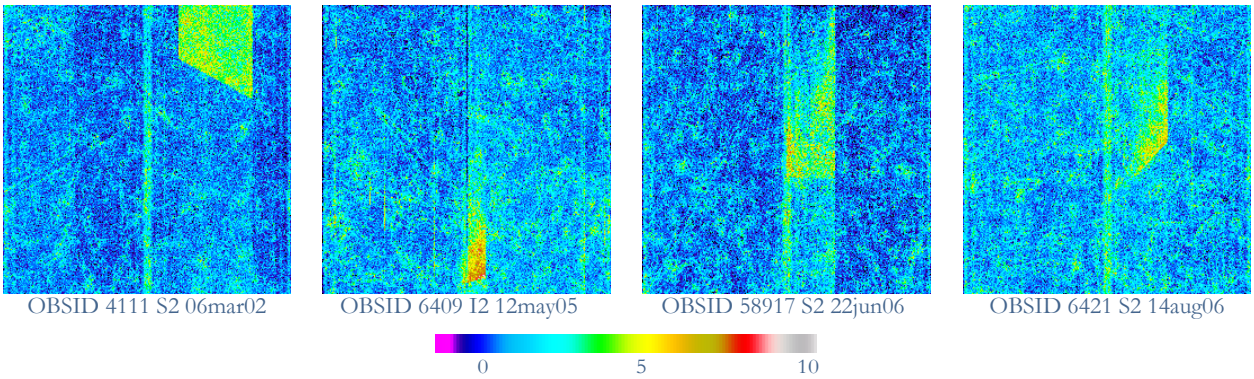

The four remaining maps are shown in Fig. 3. All possess some features in common: compact areas of bias values that are 2–6 ADU higher than normal, with boundaries that are sharply delineated by CCD column but more weakly by row. Each shows a sharp transition from anomalous to normal values at the trailing end—the farthest from the readout node—but while in the case of OBSID 58917 the transition occurs at the same row for all columns, in the other cases, the row number varies quite linearly with column, even, in thc case of OBSID 4111, across a node boundary. The slope tangents for the four trailing edges are 0.548, -0.302, 0.0, and -1.080, respectively.

The anomalous maps came from two separate CCDs, I2 and S2, connected to separate video boards, and were processed by three separate FEPs (see the table in Appendix A for details). While the BEP can in principal alter the contents of a bias map via the FEP-BEP memory-mapped interface, it is most unlikely to have caused these artifacts. No similar case of FEP memory corruption has ever been seen. Since all FEPs execute identical code, it is unlikely that they produced these artifacts, especially since the high-valued regions are aligned on abrupt, but seemingly random, column boundaries. Similarly, the cause is unlikely to be found in the video boards, either in their clocking sections or in their A-D converters, since they operate on the 4 output nodes separately and cannot therefore introduce artifacts that span node boundaries at systematically varying column values. This leaves the CCDs themselves.

3 The Bias Map Computation

To think of conditions in which the CCDs could have produced the artifacts, it is first necessary to understand how the FEPs process the raw exposure frames into bias maps. Although several algorithms have been implemented in FEP software, only one has been used since launch. It is described in detail in Applicable Document 2. Briefly, the FEP executes the following steps:

1. Reads the pixel stream from a single CCD exposure frame into the 1024x1024 pixel bias array.
2. Loops a total of 10 times (9 for OBSIDs 58917 and 6421) over the following pair of steps:
   a) Reads another CCD frame into the 1024x1024 pixel image array.
   b) Replaces each bias pixel with the corresponding image pixel if the latter is smaller.
3. Applies a median filter to the bias array, replacing any pixel that is more than 20 ADU less than at least 7 of its 8 neighbors with the median of those 8 values.
4. Loops 16 times over the following 3 steps:
   a) Reads another CCD frame into the 1024x1024 pixel image array.
   b) Marks each pixel in the image array that is more than 50 ADU larger than the corresponding pixel in the bias array.
   c) Locates each pixel, value p, in the image array that is less than 20 ADU larger than the corresponding bias array value, b, and is not contiguous to any pixel that was marked in step 4b, and replaces b with $(i*b + p + i/2)/(i+1)$, where the loop index i runs from 1 through 16.

The CCD frames that are used in these steps are not necessarily taken from consecutive CCD exposures, since the time taken by the FEP to execute one of the above steps is usually longer than the frame readout time. Although the precise number of dropped frames is not reported, in the case of the 4 anomalous maps, step 2 will typically discard 3 frames for each one used, and step 4 will drop between 7 and 9 frames, depending on the level of background noise. For typical 3.2 second exposures, allowing 30 seconds for step 3, it takes between 650 and 760 seconds for the FEPS, running simultaneously, to create their bias maps.

All pixel values are represented by 12-bit unsigned integers and arithmetic operations are performed in 32-bit signed arithmetic. Any overall drift in pixel values. *e.g.,* while the video boards warm up, is compensated within the FEP by averaging the CCD overclock values reported by each video output node. All comparisons of image and bias array values are corrected by the difference between the overclock averages of the current CCD frame and those of the frame that was read during Step 1.

Since successive readouts of a given CCD pixel will vary by only a few ADU unless an x-ray or charged particle deposits extra energy into it (or unless charge traps in the silicon emit electrons as the readout charge is moved through their location), Steps 1 and 2 result in an array of bias values that are, on average, a few ADU below the mean readout values of their corresponding CCD pixels. Occasionally, a highly charged pixel causes a video board's A-D converter to saturate (see Fig. 4) and then report an anomalously low value for the following pixel—hence Step 3, which identifies and "repairs" these rare situations which would otherwise cause the low-valued pixel to be treated as "hot" or "flickering" until the bias map was recalculated. After Step 3, the bias array elements are close approximations to the desired values, and can be used in Step 4, first to identify and ignore pixels with extra charge, and then to use the remainder to improve the bias array.

An error in the design of Step 4 might well have led to bias maps with diagonal borders between systematically higher- and lower-valued pixels. For instance, if Steps 4b and 4c had been executed within the same loop over pixels, a bias value updated in Step 4b could have affected the decision in Step 4b when it examined the following row. To avoid this possibility, Step 4b operates on the entire image array before Step 4c starts. In any case, such a feedback mechanism would be expected to generate a sloping border whose tangent was a rational number, not the apparently arbitrary values reported in Section 2.

4 Raw Frames

To see whether a similar anomaly was visible in any of the CCD frames downlinked in raw mode, we examined a subset of the 292712 downlinked raw frames in which more than 25% of their pixels possessed valid values (from 1 to 4093.) This reduced the number of images to be inspected to a manageable 4348, comprising 2194 in timed-exposure mode, 412 in continuous-clocking mode, and 1742 in special calibration modes, *e.g.*, "squeegee", "cuckoo", and "charge injection". The raw frames were transformed into GIF images in a fashion similar to that described for bias maps in Section 2, but since the overclock values themselves had been downlinked, their median was subtracted, rather than their average which had been computed onboard.The raw frames from front-illuminated CCDs showed three major types of artifact, as illustrated in Fig. 4: a) charge blooms from electron cascades, depositing thousands of ADU in compact regions; b) charge emitted by long-term traps, producing white streaks trailing down from their originating charge cloud; and c) saturation of a DEA's A/D converter—again, the result of an intense charge bloom—which causes the converter to report values that are systematically lower by several ADU while it recovers with a typical time constant of tens to hundreds of milliseconds.

A cursory inspection of the raw frames failed to show any regions of elevated pixel values whose shapes corresponded to those in Fig. 3, but since some 460,000 frames were used to create the 28695 timed exposure maps, in which there were only 4 anomalies, the probability of finding a direct example within a set of only 2194 raw frames (or 3936 frames if we add the special calibrations) was very small.[1] However, at the August 30th meeting of the ACIS Science Operations Team, Catherine Grant reported that she had identified a similar phenomenon in a handful of these same 2194 frames, as shown in Fig. 4. These effects span fewer CCD columns than do the bias map anomalies, and they don't cross node boundaries, but they possess the same straight-line boundaries in their borders facing away from the output nodes and their elevated pixel values extend over a large number of columns with only a gradual reduction in value.

The explanation for the raw-frame anomalies advanced by Catherine, and also favored by Mark Bautz, is that an energetic cosmic ray creates a charge shower spanning many pixels—running along the straight edge of the artifact. Subsequent pixel clocking will distribute the charge over many rows in the direction of the output nodes, but some of the charge will leak into traps in regions not traversed by smaller charge packets during readout. If a sufficient number of these traps possess long time constants, they will emit their charge over subsequent CCD frames.

1. Raw mode has frequently been used to monitor restricted regions of a CCD, *e.g.*, in the neighborhood of optically bright images (Vega and Betelgeuse), or narrow column strips (when mapping charge traps). These regions are too small for our purposes. Examining all 292712 raw frames is impractical and probably senseless: the 3936 frames that were checked totalled 41% of the pixels downlinked since launch in all raw modes.

5 Discussion

How could a FEP have created the 4 bias maps using the algorithm described in Section 3? There are two possibilities: either those pixels were systematically high, by 2–6 ADU, in *each* frame read by the FEP, or they were much higher than this, but only in a fraction of the 16 frames examined in step 4 of the algorithm. In the former case, it is surprising that this condition didn't persist after the bias map was created—the evidence from the corner pixels from each of the 4 runs, and illustrated for OBSID 4111 in the right-hand image in Fig. 1, is that the anomaly had disappeared by the time that events were processed, although the data do not rule out the possibility that it was still present at the start of event processing. If, however, the anomaly could not have been restricted to a *single* frame since the averaging in step 4c of the bias algorithm, repeated over 16 frames, would have reduced the original anomaly by a factor of approximately $1/n$, where $n \leq 16$, so the aberrant pixel values would have ranged from 2*16 to 6*16, and would therefore have been discarded from step 4c.

Examining the 7 raw frame anomalies displayed in Fig. 4, only OBSID 59671 at the top right covers an area that is comparable to those of the bias anomalies, but its pixel values—on average, 5 ADU above mean—would, if they persisted over 10 frames, lead to a bias map similar to those of Fig. 3. However, as described in Section 3, those 10 frames would be spread over 250–300 seconds, so for this explanation to hold, there would need to be a substantial number of charge traps whose emission time constants were of this magnitude.

Figure 4: Regions from raw frames containing anomalies that resemble those in the bias maps. The readout node is at the top, and each region is 150 pixels wide.

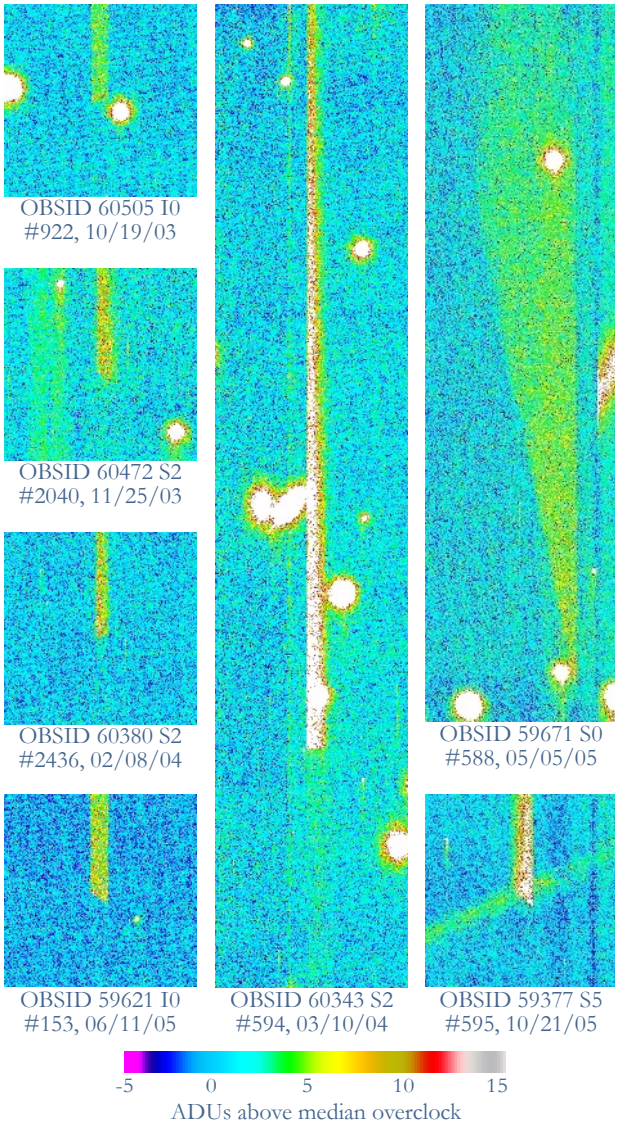

6 Conclusions and Recommendations

Thus far, the only plausible explanation for the bias map anomalies involves long-time-constant charge traps, as discussed in the preceding section. It is therefore important to confirm or refute this while keeping an open mind to other suggestions. So I propose that we pursue the following activities:

1. Examine ACIS bias maps more carefully and systematically to see whether they contain smaller scale anomalies, *e.g.,* those suggested by the raw frames of Fig. 4.
2. Look for evidence of long time constant traps in raw frames and bias maps, and study the temporal behavior of "flaring pixels," which are routinely identified by general observers with the aid of an existing *ciao* tool, to confirm that some do indeed last as long as 300–700 s.
3. Examine laboratory data, *e.g.,* from irradiated CCDs, to see whether similar artifacts have been seen or, more generally, whether evidence exists for the presence of traps with longer time constants.
4. Monitor all subsequent ACIS bias frames for artifacts similar to those of Fig. 3, since there is some indication from these 4 known instances that the frequency of the anomaly may be increasing.

7 Applicable Documents

1. ACIS Software Problem Report M06080401, August 4, 2006, available online at http://acis.mit.edu/axaf/spr/prob0139.html.
2. ACIS Software Detailed Design Document, MIT 36–53200, Release A, February 3, 2000, available online at http://acis.mit.edu/acis/sdetail/.
3. CCD Bias Level Determination Algorithms, MIT 36–56101, Version 2.1, June 19, 1995, available online at http://acis.mit.edu/axaf/model1j.pdf.

8 Abbreviations

ACIS	Advanced CCD Imaging Spectrometer
ADU	Analog data unit of pixel charge
BEP	(ACIS) Back-End Processor
CCD	Charge-Coupled Device
DDTS	(Rational™) Distributed Defect Tracking System
DEA	Digital Electronics Assembly (a.k.a. ACIS video section)
FEP	(ACIS) Front-End Processor
GIF	Graphical Image Format (© Unisys™)
OAC	Orbit Activation
OBSID	(Chandra) Observation Identifier
SI	Science Instrument
SOT	(Chandra) Science Operations Team
SPR	(ACIS) Software problem report
SSR	(On-board) Solid-State Recorder

Appendix A. Details of Bias Map Anomalies

The table is sorted by run date. Unexplained anomalies are shown in red. The remainder were due to telemetry dropouts, non-standard calibration modes, high background noise, or optical light leaks (the planet Jupiter).

obsid	starttime	targetname	seqnum	np	run	sim	otgm	mode	btmp	anomaly	CCDs
62309	1999-11-16	Faint_Mode_I	(P26B)	1	109	HRC-S	NONE	Te3x3	-109.2	Dropout	I1
62899	1999-11-17	Slow_PRAM_S1	CAP509	1	111	HRC-S	NONE	Te3x3	-109.2	CAL	S0
1	1999-11-25	JUPITER	100000	1	143	ACIS-S	NONE	Te3x3	-109.2	Jupiter	S3
62272	1999-12-13	Faint_Mode_S	DEC1299b	1	200	HRC-S	NONE	Te3x3	-109.1	Dropout	S0
811	1999-12-14	TON_S_180	700116	1	203	ACIS-S	LETG	Te3x3	-109.2	Dropout	S1
378	1999-12-30	M82	700050	1	254	ACIS-I	NONE	Te3x3	-109.2	Dropout	I1
817	1999-12-30	FIRST_J0840+363	700122	1	255	ACIS-S	NONE	Te3x3	-109.4	Dropout	S3
860	1999-12-30	NGC_3227	700165	1	256	ACIS-S	HETG	Te3x3	-109.0	Dropout	S4
62235	2000-01-08	Faint_Mode_I	DEC2699c	1	288	HRC-S	NONE	Te3x3	-109.2	Dropout	S2
386	2000-01-29	NGC_1055	700058	1	365	ACIS-S	NONE	Te3x3	-109.2	Dropout	I3
62194	2000-02-01	Faint_Mode_I	JAN3000d	2	5	HRC-S	NONE	Te3x3	-119.9	Noisy	I1,3,S2
62183	2000-02-04	Faint_Mode_I	JAN3000d	2	18	HRC-S	NONE	Te3x3	-119.9	Noisy	I1,3,S2
62168	2000-02-14	Faint_Mode_I	FEB1300c	2	55	HRC-S	NONE	Te3x3	-120.1	Noisy	I1,3,S2
62158	2000-02-23	Faint_Mode_S	FEB2000d	2	78	HRC-S	NONE	Te3x3	-119.9	Dropout	S1
62144	2000-03-01	Faint_Mode_I	FEB2700b	2	117	HRC-S	NONE	Te3x3	-119.9	Noisy	I1,3,S2
62140	2000-03-04	Faint_Mode_I	FEB2700b	2	123	HRC-S	NONE	Te3x3	-119.7	Noisy	I1,3,S2
62894	2000-04-08	Squeegee_R1	CAP591	3	9	HRC-S	NONE	Te3x3	-119.9	CAL	S0
782	2000-04-11	NGC_1569	600085	3	20	ACIS-S	NONE	Te3x3	-119.9	Dropout	I1
62084	2000-04-15	Faint_Mode_S	APR0900e	3	33	HRC-S	NONE	Te3x3	-119.7	Dropout	S3,5
62803	2000-04-15	Squeegee_R2	CAP595	3	34	HRC-S	NONE	Te3x3	-120.0	CAL	S0
62892	2000-04-16	Squeegee_R2	CAP595	3	35	HRC-S	NONE	Te3x3	-120.0	CAL	S0
62889	2000-05-01	Squeegee_R3	CAP596	3	82	HRC-S	NONE	TeRaw	-119.9	CAL	S0
62043	2000-05-28	Faint_Mode_I	MAY2100c	3	169	HRC-S	NONE	Te3x3	-119.9	Dropout	S3
62042	2000-05-30	Squeegy_L1	MAY2800c	3	178	HRC-S	NONE	Te3x3	-119.9	CAL	I0
367	2000-06-01	Q1422+231	700039	3	188	ACIS-S	NONE	Te3x3	-119.8	Dropout	S4
62030	2000-06-09	Squeegee_R5	CAP614	3	212	HRC-S	NONE	Te3x3	-119.9	CAL	S0
62023	2000-06-15	Squeegee_R6	CAP618	4	1	HRC-S	HETG	Te3x3	-119.7	CAL	S0
62019	2000-06-21	Squeegee_L2	JUN1800c	4	13	HRC-S	NONE	Te3x3	-118.5	CAL	I0
62015	2000-06-26	Squeegee_L3	JUN2500d	4	34	HRC-S	HETG	TeRaw	-119.8	CAL	I0
62876	2000-07-13	Squeegee_R7	CAP625	4	100	HRC-S	NONE	Te3x3	-120.0	CAL	S0
61987	2000-07-24	Squeegee_L5	JUL2300b	4	121	HRC-S	NONE	Te3x3	-119.8	CAL	S0
61985	2000-07-27	Squeegee_L6	JUL2300b	4	128	HRC-S	NONE	Te3x3	-119.9	CAL	S2
61981	2000-07-30	Squeegee_L7	JUL2300b	4	140	HRC-S	NONE	Te3x3	-119.9	CAL	I0
61962	2000-08-17	Squeegee_L8	AUG1300c	4	191	HRC-S	NONE	Te3x3	-119.9	CAL	I2
61946	2000-09-02	Squeegee_L10	AUG2700b	5	25	HRC-S	NONE	Te3x3	-119.9	CAL	I0
61938	2000-09-07	Squeegee_L11	SEP0300c	5	42	HRC-S	NONE	Te3x3	-120.1	CAL	S0
61932	2000-09-10	Squeegee_L12	SEP0300c	5	51	HRC-S	NONE	Te3x3	-119.9	CAL	I2
61898	2000-10-01	Squeegee_L14	SEP2800b	5	106	HRC-S	LETG	Te3x3	-119.9	CAL	I0
61896	2000-10-02	Squeegee_L15	SEP2800b	5	108	HRC-S	LETG	Te3x3	-119.3	CAL	I0
2407	2000-12-18	JUPITER	190004	6	110	ACIS-S	NONE	Te5x5	-119.9	Jupiter	S3
1904	2001-03-27	CH_CYG	300052	7	168	ACIS-S	HETG	Te3x3	-119.8	Dropout	S0
61663	2001-04-18	Faint_Mode_I	APR1701b	8	17	HRC-S	NONE	Te3x3	-119.9	Noisy	I3,S2
1560	2001-04-18	NGC4696	600117	8	18	ACIS-S	HETG	Te3x3	-119.9	Noisy	S0,2,4,5
61478	2001-09-10	Faint_Mode_I	SEP1001b	10	43	HRC-S	NONE	Te3x3	-119.9	Dropout	I1
2801	2001-12-15	PSR_0656+14	500251	11	101	ACIS-S	NONE	Te3x3	-119.4	Dropout	I2
2734	2001-12-23	GX_301-2	400214	11	123	ACIS-S	HETG	Te3x3	-119.8	Dropout	S3
3153	2002-01-14	PSS0209+0517	700592	11	180	ACIS-S	NONE	Te3x3	-119.8	Dropout	I3
61019	2002-09-26	Faint_Mode_I	SEP2302c	15	92	HRC-S	NONE	Te3x3	-117.2	Dropout	I0,S3
3004	2002-10-31	MRK_663	700443	15	192	ACIS-S	NONE	Te3x3	-119.7	Dropout	I1
60898	2003-01-02	Faint_Mode_I	DEC2502b	16	179	HRC-S	NONE	Te3x3	-119.6	Dropout	I0,1,2,S2,3
3192	2003-01-22	A2626	800192	17	10	ACIS-S	NONE	Te5x5	-119.7	Dropout	S3
3726	2003-02-24	JUPITER	100036	17	137	ACIS-S	NONE	Te5x5	-119.6	Jupiter	S3

obsid	starttime	targetname	seqnum	np	run	sim	otgm	mode	btmp	anomaly	CCDs
4418	2003-02-25	JUPITER	100036	17	139	ACIS-S	NONE	Te5x5	-119.7	Jupiter	S3
4111	2003-06-02	F15130-1958	700790	19	5	ACIS-S	NONE	Te5x5	-119.7	Artifact	S2 FEP2
60669	2003-07-06	Faint_Mode_S	JUL0103a	19	79	HRC-S	NONE	Te3x3	-116.5	Dropout	S1,3
3818	2003-08-01	OGLE-1999-BUL-3	400305	19	143	ACIS-S	NONE	Te5x5	-119.6	Dropout	S4
3933	2003-08-06	NGC_5204_X-1	600307	19	161	ACIS-S	NONE	Te3x3	-119.2	Dropout	S1
3930	2003-09-12	NGC_1705	600304	20	82	ACIS-S	NONE	Te3x3	-119.1	Dropout	S1,3
5195	2003-10-08	4C_74.26	700679	20	146	ACIS-S	HETG	Te3x3	-119.9	Dropout	S2,4
60492	2003-11-02	Faint_Mode_S	NOV0103a	21	11	HRC-S	NONE	Te3x3	-119.8	Noisy	S0,2,4,5
4756	2004-01-09	3C_388	700842	21	200	ACIS-I	NONE	Te5x5	-119.7	Dropout	I2
4696	2004-02-27	NGC_1023	600351	22	141	ACIS-S	NONE	Te5x5	-119.7	Dropout	S4
4954	2004-04-01	Centaurus_Cluster	800401	23	40	ACIS-S	NONE	Te3x3	-119.7	Dropout	I2
5130	2004-04-09	“E0102-72[S3,-12”	590328	23	59	ACIS-S	NONE	Te5x5	-119.7	Dropout	S4
4915	2004-05-07	LEDA_1613994	700996	23	126	ACIS-S	NONE	Te3x3	-119.7	Dropout	I2
4682	2004-05-23	M31-Center	600337	24	27	ACIS-I	NONE	Te3x3	-119.5	Dropout	I0
60132	2004-07-15	Faint_Alt_I	JUL1204b	24	167	HRC-S	NONE	Te3x3	-119.7	Dropout	I3
4938	2005-05-03	RCS2318.5+0034	800389	29	147	ACIS-S	NONE	Te5x5	-119.7	Noisy	S2
7063	2005-10-20	VV_114	600501	32	40	ACIS-S	NONE	Te5x5	-119.7	Noisy	I3,S4
6409	2005-12-15	DG_Tau	200384	33	51	ACIS-S	NONE	Te5x5	-119.7	Artifact	I2 FEP5
7058	2006-06-07	NGC7265	600496	35	146	ACIS-I	NONE	Te5x5	-119.7	Noisy	I0,2,3
58917	2006-06-22	Faint_Mode_I	JUN1906b	36	32	HRC-S	HETG	Te3x3	-117.0	Artifact	S2 FEP5
6421	2006-08-07	M17_Pointing_I	200395	36	164	ACIS-I	NONE	Te5x5	-119.6	Artifact	S2 FEP0